

Tilted Janus polymer pillars†

Myoung-Woon Moon,^a Tae-Gon Cha,^{ab} Kwang-Ryeol Lee,^a Ashkan Vaziri^{*c} and Ho-Young Kim^{*b}

Received 18th March 2010, Accepted 28th April 2010

DOI: 10.1039/c0sm00126k

Asymmetric adhesion is used by many insects and gecko lizards, allowing them to move on nearly any surface – horizontal, tilted or vertical. The feet of many of these creatures is covered with intricate fibrillar structures that are responsible for their superb manoeuvring ability. Among these creatures, gecko lizards have one of the most efficient and interesting adhesion devices consisting of finely angled arrays of branched fibers (setae). Here, we developed a method to create tilted Janus (two-face) micropillars on the surface of an elastomeric polymer to mimic the geometry of a gecko's footpad. The method combines soft lithography to create straight micropillars and ion beam irradiation to tilt the straight micropillars in a controlled fashion. A set of experiments were performed to measure the adhesion and friction characteristics of the fabricated tilted micropillars. Our experiments showed that the friction force along the tilting direction is approximately three times higher than the friction force associated with the sliding against the tilting direction of tilted micropillars due to the difference in the contact area during sliding of a glass ball.

1. Introduction

The footpad of many insects, such as water striders, flies, spiders and gecko lizards, are covered with fibrillar structures, giving them the ability to live on water or climb smooth and rough surfaces.^{1–5} These fibers bend and conform to the surface roughness, creating very high number of contact points and, thus, large contact areas. Among these creatures, the gecko's footpad has the highest density fibrillar structures forming one of the most efficient adhesion systems in nature.^{5–8} At the micron scale, the gecko's footpad is covered with hundreds of thousands of protruding hair-like structures called setae (see Fig. 1A), which are responsible for the gecko's superb climbing abilities.^{7–9} In this work, we developed a simple technique for fabrication of tilted polymer micropillars that mimics a gecko's footpad structure by exposing straight micropillars to an ion beam. Our work complements previous efforts for fabricating fibrillar structures,^{5–9} which provided structural organizations that mimic the gecko's footpad and help evaluate some of the intricate properties of geckos' footpads under controlled experimental conditions.^{10–20} Fig. 1B shows schematics of the five steps involved in the creation of the tilted micropillars. First, we fabricated straight micropillars on the surface of the polydimethylsiloxane (PDMS) using soft lithography (steps 1–4 in Fig. 1B). After fabrication of the straight pillars, Ar⁺ broad ion beam irradiation was used to tilt the micropillars. The outcome is an array of micropillars that are uniformly tilted towards the ion beam irradiation direction. Fig. 1C shows the polymer

micropillars prior to and after 20 min exposure to an ion beam with an incident angle of 90° (parallel to the surface of the polymeric substrate). In Fig. 1C, the micropillars have a diameter of 9.3 μm, height of 30 μm and spacing of 10 μm, where spacing is defined as the distance between the edges of the adjacent micropillars (*e.g.* the center-to-center distance of the micropillars in this case is 19.3 μm). This configuration gives a density of ~2700 mm⁻², which is approximately five times lower than the setae density on the gecko's footpad.^{7,21,22} The gecko's setae are approximately 110 μm in length, which is 3 times longer than the created pillars and 5 μm in diameter.⁷ The developed technique can be used to fabricate micropillars with a wide range of dimensions and spacing with the lower limit of spacing and diameter of ~1 μm.²³

2. Method and materials

Fabrication of straight micropillars

Uniform straight micropillars were created using soft lithography on a surface area 4 × 4 cm² of a PDMS coupon. First, the SU-8 of photoresist (PR) on Si wafer was spin-coated with 30 μm Cr mask and used to fabricate the negative shape of pattern mask (Fig. 1B – step 1). The wafer was heated on a hot plate in two steps at 60 °C and 90 °C for 10 min each. Cr masks were placed on solidified PR, aligned with EVG 6200 mask aligner and exposed to UV (EVGroup, Austria). The exposed PR was developed and cleaned with isopropyl alcohol. PDMS networks were prepared by mixture of elastomer and cross-linker in a mass ratio of 10 : 1 (Sylgard-184, Dow Corning, MI). The mixture was poured on a pre-patterned PR mold (Fig. 1B – step 3). The trapped air bubbles were removed in a vacuum chamber. The samples were cured on a hot plate at 75 °C for 75 min, resulting in cross-linked PDMS network with straight micropillars (Fig. 1B – step 4). Microscopic images of micropillar structures were acquired using a scanning electron microscope (SEM, Nova-SEM, FEI Company).

^aConvergence Technology Laboratory, Korea Institute of Science and Technology, Seoul, 130-650, Republic of Korea

^bSchool of Mechanical and Aerospace Engineering, Seoul National University, Seoul, 151-744, Republic of Korea. E-mail: hyk@smu.ac.kr

^cDepartment of Mechanical and Industrial Engineering, Northeastern University, Boston, MA, 02115, USA. E-mail: vaziri@coe.neu.edu

† Electronic supplementary information (ESI) available: Appendices 1–3. See DOI: 10.1039/c0sm00126k

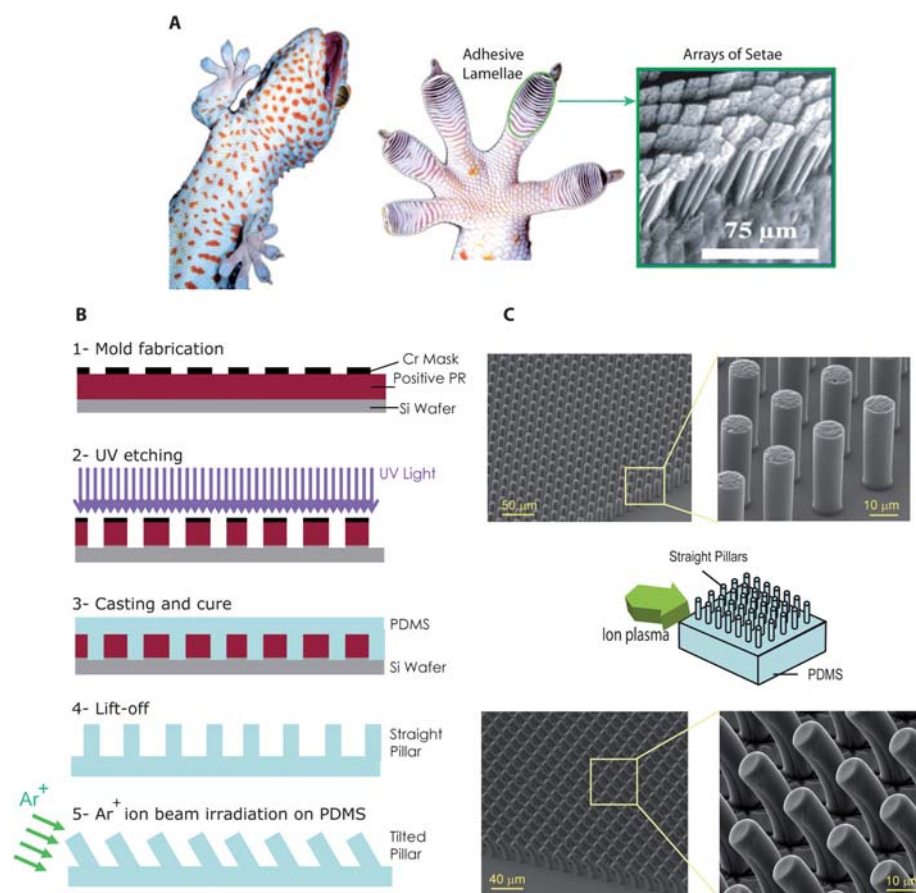


Fig. 1 Bioinspired titled micropillars fabricated on PDMS. (A) Hierarchical Gecko's footpad structure. The left image shows a ventral view of a tokay gecko (*G. gecko*) climbing a vertical glass. The middle image shows a ventral view of a footpad, with adhesive lamellae (scansors) visible as overlapping pads.¹⁵ The proximal portion of a single lamella, with individual setae in an array is shown in the right image. (B) A schematic of the fabrication process. The straight (non-tilted) micropillars are fabricated on the PDMS surface using soft lithography (steps 1–4). The straight micropillars to tilt uniformly towards the ion beam irradiation direction (step 5), resulting in a uniform array of tilted micropillars. (C) Straight (top) and tilted (bottom) micropillars fabricated using the developed fabrication process. The micropillars have a diameter of 9.3 μm , height of 30 μm and spacing of 10 μm . The straight micropillars were tilted $\sim 27^\circ$ using ion beam irradiation with an incident angle of 90° (as shown, schematically) and a treatment duration of 20 min.

Ion beam irradiation

The straight micropillars were subject to Ar^+ ion beam irradiation using a hybrid ion beam system (Fig. 1B – Step 5). In this experiment, PDMS substrates decorated with straight micropillars fabricated on their surface were placed on a tilted die at a certain angle in the vacuum chamber. The chamber had the working pressure $\sim 10^{-5}$ Pa. The ion beam treatment was made with argon discharge at an anode voltage of 1 keV, a bias voltage of -600 V and a pressure of 0.49 Pa. The tilting angle of the micropillars was defined as the tangential angle at the tip of micropillars and was measured from the side view SEM images of micropillars.

Adhesion measurement

The adhesion force of micropillars against a steel ball was measured using a tensiometer (DCAT 21, Dataphysics, Germany). In the experiments, first, the stage was moved upwards and the PDMS coupon came into contact with the steel ball with a diameter 6 mm. The stage then moved upward at constant speed ($10 \mu\text{m s}^{-1}$) while the force was measured at a frequency of 50 Hz by

a sensor at a resolution of $1 \mu\text{N}$. As the force reached a predefined load, or preload, the stage was set to move downward at a constant speed ($10 \mu\text{m s}^{-1}$), while the force was measured by the sensor.

Friction measurement

The directional friction behavior of the tilted micropillars against a glass ball of 4 cm in diameter was measured using a custom-made device. Prior to each experiment, the glass ball was cleaned with isopropyl alcohol and blown with N_2 gas. The friction force of a PDMS coupon covered by straight or tilted micropillars was measured at a frequency of 64 Hz using a sensor at a resolution of $50 \mu\text{N}$ as the glass ball slides over the coupon surface. The sliding distance was set to 1 mm at a constant speed of $2 \mu\text{m s}^{-1}$. The measured friction force in the steady sliding regime was divided by the normal force to estimate the average coefficient of friction.

3. Results and discussion

Fig. 2A shows the detailed structure and surface morphology of the tilted micropillars fabricated using the technique shown in

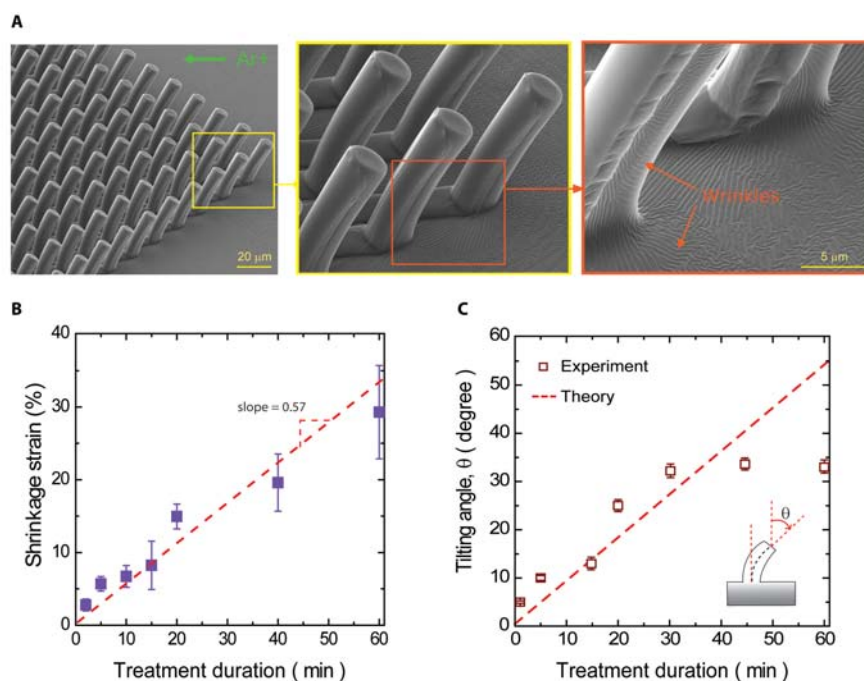


Fig. 2 The mechanics of micropillar tilting. (A) SEM images of the tilted micropillars, showing wrinkles on the surface of the micropillars and the polymeric substrate. (B) The shrinkage strain of the PDMS *versus* the treatment duration. The data shown is the average of at least 5 measurements. (C) The dependence of the micropillars tilting angle on the treatment duration for ion beam with an incident angle of 90° . The estimation of the tilting angle based on the measured shrinkage strain is also shown and denoted by ‘Theory’. The inset shows the definition of tilting angle of each micropillar.

Fig. 1B. The ion beam irradiation generates wrinkles on the polymer surface, as well as the side of the micropillars that is exposed to ion beam. The ion beam irradiation causes surface modification of the PDMS and induces a stiff skin, which is 70–100 times stiffer than PDMS.^{24–26} Ion beam irradiation also causes shrinkage of the surface, resulting in a strain mismatch between the induced stiff skin and soft polymer and thus, instability of the surface skin in the form of wrinkles.²⁷ Thus, after ion beam exposure, the micropillars have two completely different surface topologies and form an array of ‘uniformly tilted Janus pillars’.

We performed a separate experiment to quantify the shrinkage strain of the polymer surface due to ion beam irradiation by exposing straight micropillars to an ion beam with an incident angle of 0° . This experiment allows estimation of the shrinkage strain of the polymer surface by measuring the reduction in the pillar diameter at the top of micropillars due to ion beam irradiation – see the ESI for details and schematic of the experiment.[†] Fig. 2B summarizes the results of this experiment, where the shrinkage strain of the polymer surface, ε , is plotted *versus* the ion beam treatment duration, t . For an ion beam with an accelerating voltage of 1 keV and a bias voltage of -600V , $\varepsilon \cong 0.57t$. Considering the deformation of a pillar subjected to surface shrinkage at one side gives a simple geometrical relationship for its tilting angle and the measured shrinkage strain, $\theta = \varepsilon \times h/d$, where d and h are the diameter and height of the micropillars, respectively. Fig. 2C shows the dependence of the tilting angle on the duration time for micropillars exposed to an ion beam with an incident angle of 90° . Tilting angle as large as 34° was achieved using the ion

beam irradiation with the aforementioned process conditions. The estimation of the tilting angle based on the measured strain is also plotted, which shows good agreement with the measured value for ion treatment duration, $t \leq 30$ min. For longer treatment durations, the side of the micropillars subjected to the ion beam appears to be etched and ion beam irradiation does not result in further shrinkage of the micropillars’ surface, thus, the tilting angle of the micropillars becomes relatively independent of the treatment duration.

Fig. 3 shows the effect of ion beam incident angle on the tilting angle of the micropillars. Fig. 3A shows examples of the tilted micropillars subjected to two different ion beam incident angles, 60° and 90° and Fig. 3B shows the dependence of the micropillars’ tilting angle on the ion incident angle, denoted by α for ion treatment of 60 min. Fig. 3C expands these results for various treatment durations. An ion beam normal to the micropillars and parallel to the surface (*i.e.* $\alpha = 90^\circ$) leads to the largest tilting angle. Ion beam normal to the polymer surface and parallel to the straight micropillars (*i.e.* $\alpha = 0^\circ$) results in almost no tilting of the micropillars after 20 min of irradiation. The examination of the morphology of the tilted pillars indicates that the height of the micropillars, where surface wrinkles appear, depends on the ion incident angle. For large incident angles, surface wrinkles appear along the total height of the micropillars, as shown for $\alpha = 90^\circ$ in Fig. 2A and 3A. For smaller ion incident angles, surface wrinkles appear only on the upper part of the micropillars and the bottom part of the pillars does not get exposed to the direct ion beam due to the shadowing effect of other micropillars. This leads to a smaller tilting angle at a lower ion beam incident angle.

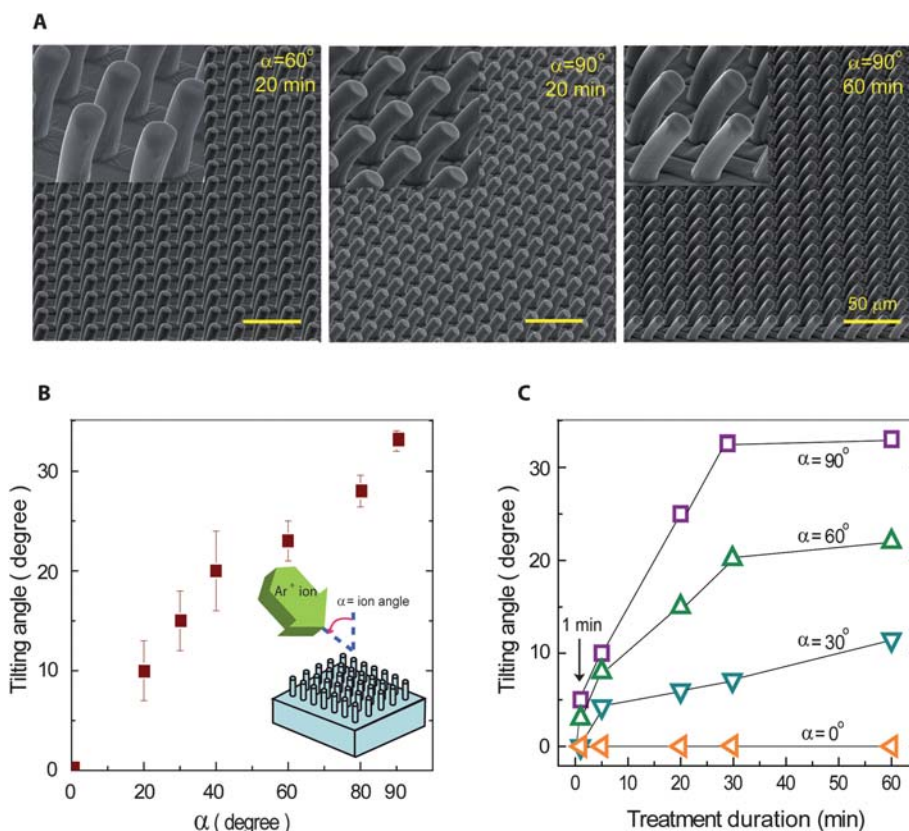


Fig. 3 The role of ion beam incident angle. (A) SEM images of tilted micropillars with different treatment conditions. (B) Micropillars' tilting angle *versus* the ion incident angle for a treatment duration of 60 min. Inset: a schematic of the angled ion incidence. (C) The tilting angle *versus* the treatment duration for four different incident angles of ion beam.

Adhesion measurement

Next, we examined the adhesion characteristics of a polymeric surface covered by tilted micropillars in two separate experiments. In the first experiment, the adhesion strength of straight and tilted micropillars was measured using a tensiometer – see Fig. 4A for a schematic of the experiment. In this experiment, the micropillars come into contact with the steel ball during the *advancing* stage, while the contact force is measured by the sensor. During the *receding* phase, the measured force exhibits values larger than zero (tensile) prior to a sudden drop to zero, which denotes the loss of contact between the steel ball and the polymeric surface covered by micropillars. The maximum value of positive force denotes the pull-off strength of the surface – see Fig. 4B and its inset. In the results shown in Fig. 4B, the maximum preload, ~ 11 mN, is reached at the maximum advancing displacement of 0.2 mm and the pull-off load (P) is ~ 0.05 mN for micropillars with tilting angles of 32° . We carried out the adhesion experiment for straight and titled micropillars for a relatively broad range of preloading. In general, the pull-off load of a substrate covered with micropillars increases by increasing the preload and is higher for micropillars with a larger tilting angle. These observations are in qualitative agreement with the sliding-induced adhesion study carried out on the stiff polymer fiber arrays.²⁸

In Fig. 4C, we calculated the adhesion strength of the surfaces covered with straight and tilted micropillars for different

preloads between 2 and 20 mN. The adhesion strength was calculated by dividing the measured pull-off load under each preload by the maximum contact area generated due to advancing of the substrate, A_m . This area is estimated as $A_m = N \cdot \pi r^2$, where N is the number of micropillars in contact with the indenter and r is the radius of the micropillars. In this calculation, N is related to the indentation depth associated with each preload, using a simple geometrical relationship.^{18,29} The results are presented in Fig. 4C for straight and tilted micropillars. As discussed before, ion beam irradiation caused surface modification and shrinkage, and result in appearance of surface wrinkles and possible change in surface energy and stiffness. In Fig. 4C, we presented results for straight pillars subjected to an ion beam at an incident angle of $\alpha = 0^\circ$ with three different treatment durations (5, 10 and 30 min). No significant difference was observed between the adhesion strengths of the straight micropillars, suggesting that ion beam irradiation duration and the corresponding alterations in the surface properties do not have a considerable effect on the surface adhesion properties. In this experiment, the tilting angle of the micropillars was controlled by changing the treatment duration, while the preload is varied by changing the receding displacement. The polymer substrate covered with tilted micropillars, with a tilting angle of 32° , has an adhesion strength that is approximately one order of magnitude higher than the adhesion strength of substrates covered by straight pillars with the same geometry

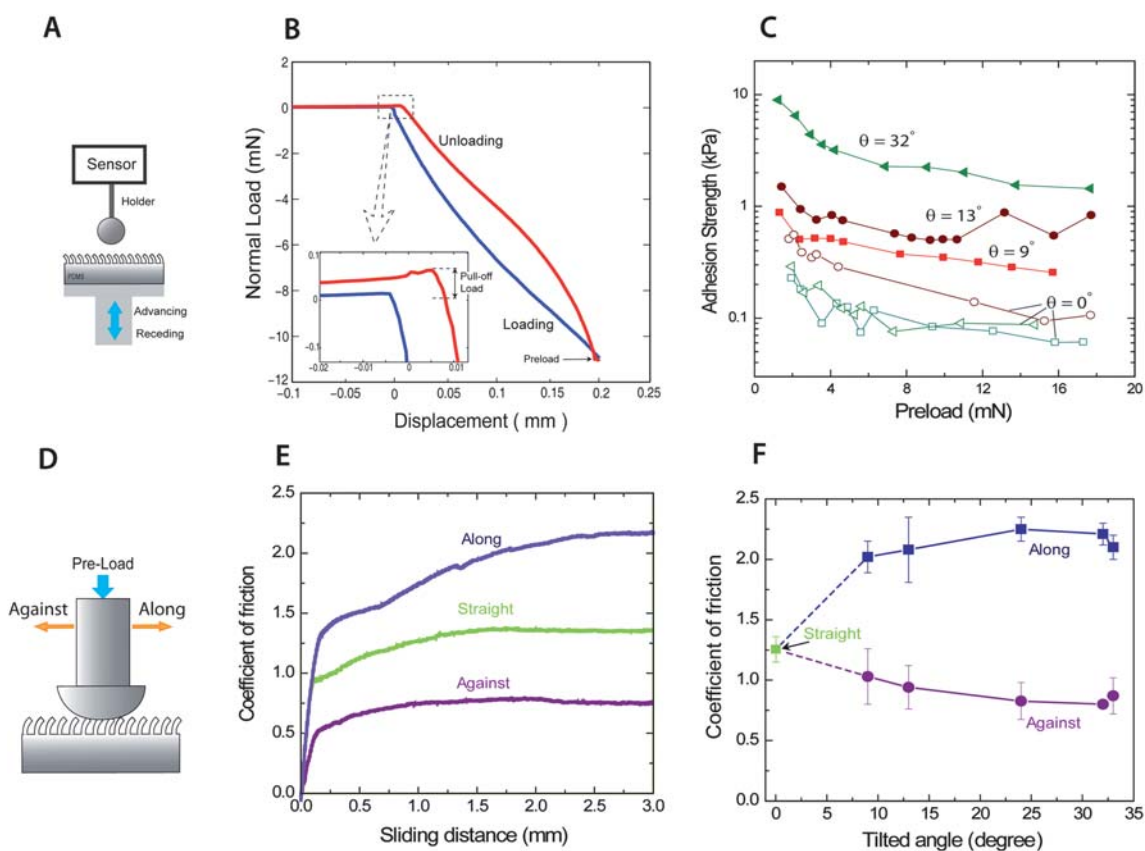


Fig. 4 Adhesion and friction experiments. (A) A schematic of the adhesion experimental setup. (B) The force–displacement response of PDMS substrates covered with straight micropillars and tilted micropillars. Inset: A magnified image demonstrating the pull-off load achieved prior to losing the contact. (C) The adhesion strength and adhesion energy *versus* the preload for PDMS substrates covered with straight pillars, $\theta = 0^\circ$, and tilted pillars with various tilting angles denoted by θ . For straight micropillars, three sets of results are presented, which correspond to three different treatment durations of 5 min (open squares), 10 min (open circles) and 20 min (open triangles). (D) A schematic of the friction experimental setup. (E) The friction force–displacement response of PDMS substrates covered with straight micropillars and tilted micropillars for sliding along and against the tilting direction. In this set of experiments, the treatment duration was 30 min for both straight and tilted pillar arrays, the normal force (denoted as pre-load in Fig. 4D) was 400 mN and the glass ball with a diameter of 2 cm was moved at a constant velocity of $5\ \mu\text{m s}^{-1}$. (F) The coefficient of friction *versus* the tilting angle for sliding along and against the tilting direction.

and density at the same pre-loading. The adhesion strength of a substrate covered with micropillars is higher for micropillars with a larger tilting angle. These observations are in qualitative agreement with the sliding-induced adhesion study carried out on the stiff polymer fiber arrays.²⁸ In contrast, the adhesion strength of both straight and tilted pillars gradually decreases with an increase in the pre-load.²⁸ The gecko's setae have an average adhesion stress of 30 kPa,³⁰ which is relatively higher than the maximum adhesion strength (~ 10 kPa) measured for the tilted micropillar array, however, the synthetic micropillar array has a lower density compared to the gecko's array of setae.

Asymmetric friction behavior of titled micropillars

Directional friction behavior of the tilted micropillars against a glass ball was measured using a custom-made setup, shown schematically in Fig. 4D. The friction force was measured by moving the glass ball *along* and *against* the pillar tilting direction and was compared to the friction force of surface covered with straight pillars, which were subjected to normal ion beam

irradiation with a duration of 30 min prior to the friction experiment, see Fig. 4E. In the early stages of the experiment, the friction force for sliding against the tilting direction was lower than the friction force of straight pillars, as well as that of sliding along the tilting direction. After this initial stage, the friction force at the steady state regime was considerably lower for sliding against the pillar direction compared to the friction forces for straight micropillars and for sliding along the pillar direction under the same test condition. This observation is consistent with the behavior of a gecko's footpad,^{31,32} as well as the measurement on biologically inspired synthetic fibrillar surfaces.^{13,32} The friction force for sliding along the pillar direction is also higher than the friction force of the straight micropillars due to the considerably higher associated adhesion strength and a larger contact area for this configuration, as demonstrated in the previous section and the ESI (see Fig. S2).[†] This observation is also consistent with previous measurements on fibrillar surfaces.^{10,32}

The direction-dependant friction behavior of titled pillars is further studied in Fig. 4F, where we studied the role of the micropillars' tilting angle on the substrate coefficient of friction. In each experiment, the coefficient of friction of the substrates

was estimated by dividing the average friction force by the normal force in the steady state sliding regime. The friction force along the tilting direction is about three times higher than the friction force associated with the sliding against the tilting direction of the micropillars. The coefficient of friction for sliding along the tilting direction of the micropillars is considerably higher than that of the straight pillars. At this sliding velocity, no significant sensitivity to the tilting angle was observed. This could be due to the similar increase of contact area as a glass ball slides over the pre-tilted micropillars with the tilting angle $>10^\circ$. To examine the role of the sliding velocity on the friction behavior of the tilted micropillars, we carried out the friction experiment for a wide range of sliding velocities – see Fig. S3 in the ESI.† Our results show that the coefficient of friction (COF) for sliding along the tilting direction of micropillars minimally depends on the sliding velocity, which is consistent with the behavior observed for stiff polymer fiber arrays.²⁹ In contrast, the COF for sliding against the micropillar tilting direction decreases remarkably at higher sliding velocities. Sliding against the tilting direction is accompanied by significant mechanical deformation of micropillars and thus, the inherent time-dependant behavior (*i.e.* visco-elasticity) of polymeric micropillars influence the friction behavior of the micropillars, leading to a strongly rate-dependant behavior.

4. Conclusions

We have developed a robust method to create an array of uniformly tilted micropillars on the surface of PDMS that resembles geckos' setae. The developed technique provides novel avenues for enhancing the functionality of synthetic hair-like and micropillar structures, as investigated in this article by performing an assay of controlled adhesion and friction experiments. Potential applications of the created structures are vast and range from non-wetting painting and smart adhesives^{33–38} to bioinspired machines such as nano- and micro- robots with climbing abilities.^{39,40}

Acknowledgements

We thank Prof. J. W. Hutchinson from Harvard School of Engineering and Applied Sciences and the anonymous reviewers for their constructive comments and suggestions. This work was supported in part by a grant of 2E21580 from KIST project (MWM, KRL) and by a NRF grant no. 2007-412-J03001 and 2009-0067974 (HYK), and in part by the U.S. Air Force Office of Scientific Research under AFOSR YIP grant, under award number FA 9550-10-1-0145 (AV).

The authors declare no conflict of interest.

References

- 1 L. Cheng, *Nature*, 1973, **242**, 132–133.
- 2 R. F. Foelix, *Biology of Spiders*, Harvard Univ. Press, Cambridge, UK, 1984.
- 3 V. B. Wigglesworth, *J. Exp. Biol.*, 1987, **129**, 373–376.
- 4 R. B. Huey and P. E. Hertz, *J. Exp. Biol.*, 1982, **97**, 401–409.
- 5 H. Gao and H. Yao, *Proc. Natl. Acad. Sci. U. S. A.*, 2004, **101**, 7851–7856.
- 6 A. P. Russell, *J. Zool.*, 1975, **176**, 437–476.
- 7 W. R. Hansen and K. Autumn, *Proc. Natl. Acad. Sci. U. S. A.*, 2005, **102**, 385–389.
- 8 H. Gao, X. Wang, H. Yao, S. Gorb and E. Arzt, *Mech. Mater.*, 2005, **37**, 275–285.
- 9 Y. Tian, N. Pesika, H. Zeng, K. Rosenberg, B. Zhao, P. McGuiggan, K. Autumn and J. Israelachvili, *Proc. Natl. Acad. Sci. U. S. A.*, 2006, **103**, 19320–19325.
- 10 M. P. Murphy, B. Aksak and M. Sitti, *Small*, 2009, **5**, 170–175.
- 11 B. Aksak, M. P. Murphy and M. Sitti, *Langmuir*, 2007, **23**, 3322–3332.
- 12 T. Kim, H. E. Jeong, K. Y. Suh and H. H. Lee, *Adv. Mater.*, 2009, **21**, 2276–2281.
- 13 S. Kim and M. Sitti, *Appl. Phys. Lett.*, 2006, **89**, 261911.
- 14 B. Chen, P. Wu and H. Gao, *J. R. Soc. Interface*, 2009, **6**, 529–537.
- 15 A. P. Russell and T. E. Higham, *Proc. R. Soc. London, Ser. B*, 2009, **276**, 3705–3709.
- 16 H. E. Jeong, J.-K. Lee, H. N. Kim, S. H. Moon and K. Y. Suh, *Proc. Natl. Acad. Sci. U. S. A.*, 2009, **106**, 5639–5644.
- 17 M. Varenberg, A. Peressadko, S. Gorb and E. Arzt, *Appl. Phys. Lett.*, 2006, **89**, 121905.
- 18 A. J. Crosby, M. Hageman and A. Duncan, *Langmuir*, 2005, **21**, 11738–11743.
- 19 N. J. Glassmaker, A. Jagota, C.-Y. Hui and J. Kim, *J. R. Soc. Interface*, 2004, **1**, 23–33.
- 20 M. Varenberg and S. Gorb, *J. R. Soc. Interface*, 2007, **4**, 721–725.
- 21 R. Ruibal and V. Ernst, *J. Morphol.*, 1965, **117**, 271–293.
- 22 W. Sun, P. Neuzil, T. S. Kustandi, S. Oh and V. D. Samper, *Biophys. J.*, 2005, **89**, L14–L17.
- 23 E. Delamarche, H. Schmid, B. Michel and H. Biebuyck, *Adv. Mater.*, 1997, **9**, 741–746.
- 24 M.-W. Moon, S. H. Lee, J. Y. Sun, K. H. Oh, A. Vaziri and J. W. Hutchinson, *Proc. Natl. Acad. Sci. U. S. A.*, 2007, **104**, 1130–1133.
- 25 M.-W. Moon, S. H. Lee, J. Y. Sun, K. H. Oh, A. Vaziri and J. W. Hutchinson, *Scr. Mater.*, 2007, **57**, 747–750.
- 26 M.-W. Moon, E. K. Her, K. H. Oh, K. R. Lee and A. Vaziri, *Surf. Coat. Technol.*, 2008, **202**, 5319–5324.
- 27 M.-W. Moon and A. Vaziri, *Scr. Mater.*, 2009, **60**, 44–47.
- 28 J. Lee, C. Majidi, B. Schubert and R. S. Fearing, *J. R. Soc. Interface*, 2008, **5**, 835–844.
- 29 C. Greiner, A. del Gampo and E. Arzt, *Langmuir*, 2007, **23**, 3495–3502.
- 30 N. Gravish, M. Wilkinson and K. Autumn, *J. R. Soc. Interface*, 2008, **5**, 339–348.
- 31 K. Autumn, A. Dittmore, D. Santos, M. Spenko and M. Cutkosky, *J. Exp. Biol.*, 2006, **209**, 3569–3579.
- 32 H. Yao, G. Della Rocca, P. R. Guduru and H. Gao, *J. R. Soc. Interface*, 2008, **5**, 723–734.
- 33 J. Lee, R. S. Fearing and K. Komvopoulos, *Appl. Phys. Lett.*, 2008, **93**, 191910.
- 34 M. P. Murphy, B. Aksak and M. Sitti, *J. Adhes. Sci. Technol.*, 2007, **21**, 1281–1296.
- 35 L. Qu, L. Dai, M. Stone, Z. Xia and Z. L. Wang, *Science*, 2008, **322**, 238–242.
- 36 A. K. Geim, S. V. Dubonos, I. V. Grigorieva, K. S. Novoselov, A. A. Zhukov and S. Y. Shapoval, *Nat. Mater.*, 2003, **2**, 461–463.
- 37 H. Lee, B. P. Lee and P. B. Messersmith, *Nature*, 2007, **448**, 338–342.
- 38 S. Reddy, E. Arzt and A. del Campo, *Adv. Mater.*, 2007, **19**, 3833–3837.
- 39 R. J. Wood, *IEEE Trans. Rob.*, 2008, **24**, 341–347.
- 40 D. L. Hu, M. Prakash, B. Chan and J. W. M. Bush, *Exp. Fluids*, 2007, **43**, 769–778.